Experimental Demonstration of Thrust Vectoring with a Vertical Axis Wind Turbine using Normal Load Measurements

Leblanc, Bruce; Ferreira, Carlos

DOI
10.1088/1742-6596/1618/5/052030

Publication date
2020

Document Version
Final published version

Published in
Journal of Physics: Conference Series

Experimental Demonstration of Thrust Vectoring with a Vertical Axis Wind Turbine using Normal Load Measurements

Experimental Demonstration of Thrust Vectoring with a Vertical Axis Wind Turbine using Normal Load Measurements

Bruce LeBlanc and Carlos Ferreira
Delft University of Technology, Kluyverweg 1, Delft, The Netherlands
E-mail: b.p.leblanc@tudelft.nl

Abstract. The aerodynamic loading of a vertical axis wind turbine varies with the azimuth position of the blades. The thrust of the VAWT can be computed as a decomposition of the normal force on each of the blades. By varying the blade loading as a function of turbine azimuth, it is possible to vary the direction of the average thrust of the turbine. An experiment is performed using an active pitch controlled H-VAWT turbine in the Open Jet Facility at TU Delft demonstrating the ability to actively vary the rotor aerodynamic loading and as a result the average thrust vector. By applying a sinusoidal pitch actuation with phase offsets, a directional change in the average thrust vector of over 78° was demonstrated.

1. Introduction

The vertical axis wind turbine has been proposed as a potential solution for lowering the overall costs of turbine installations, especially in large floating offshore concepts [1, 2]. This is achieved through a lower center of gravity and a greater tolerance to platform motions than an equivalent horizontal axis machine. The cost of the platform system is related to the overturn moment of the turbine in crucial operational states. The largest contribution to this moment is the rotor thrust. It has been shown that the orientation of the thrust vector for a VAWT can be directed by varying the blade normal loads as a function of azimuth in specific ways [3]. The ability to change the thrust vector dynamically without having to yaw the machine can have many positive benefits in the field of wind farm control. As the thrust vector changes dynamically with the rotation as well, it may be possible to actively shape this vector to control side to side loading for fatigue reasons, or to bias one side or the other for the effects of wake steering.

In this work, an experiment with active control of turbine pitch has been performed demonstrating that the azimuthally integrated thrust load can be altered. As a proof of concept, an open-loop system of sinusoidal pitch activation with changing phase offset is demonstrated. The measured normal loading of the turbine in a zero pitch baseline configuration is discussed and compared to the actively varying sinusoidal pitch. In future work, closed-loop control of the rotation averaged or real-time normal loading could be used to actively tailor loading as required for the given aim.

1.1. Definition of Terms

The coordinate system used for the discussion and analysis is given in figure 1. Wind consistently comes from the 90° azimuth position, with the X direction following the direction of the wind. The turbine rotates counter-clockwise, and the Y direction is defined using the right-hand rule.

The blade pitch, β, sign convention is given in figure 2. The curved path of the airfoil is shown with a dashed line. Positive turbine pitch is defined as pitching in toward the center of rotation, which corresponds to an increase in angle of attack for each azimuth position. Negative blade pitch therefore corresponds to a decrease in α in comparison to the expected geometric angle of attack in a constant wind. Equation 1 is used to define blade pitch as a function of azimuth angle θ, phase offset ϕ and a fixed pitch offset β_0 for this study, β_0 is kept at a constant 0°.

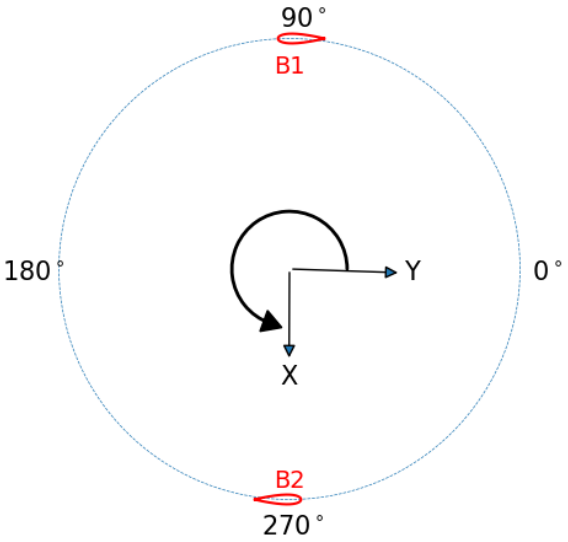

Figure 1. Turbine coordinate system

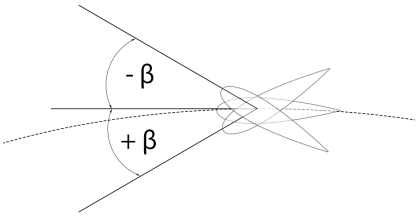

Figure 2. Blade pitch angle sign convention

$$\beta = A\sin(\theta + \phi) + \beta_0 \tag{1}$$

2. PitchVAWT Turbine

The turbine is a two-bladed H-shaped vertical-axis turbine with two horizontal struts per blade located at approximately 25 % and 75 % of the blade length to reduce deflection during operation. The rotor has a radius of 0.75 m, with a chord length of 0.075 m giving a chord to radius ratio of 0.1, thereby minimizing the effects of flow curvature and unsteady aerodynamics. The general specifications can be seen in Table 1. The PitchVAWT turbine is shown in figure 3. More detail on the design is given in previous works, [4, 5]. The pitch of each blade of the turbine is controlled by an independent motor and can therefore be configured to test most conceivable pitch schemes in the relatively controlled environment of the Open Jet Facility at the Delft University of Technology. Operating ranges for the turbine are limited by pitch rate to 364 $^\circ\,\mathrm{s}^{-1}$ or for fixed pitch applications to 350 rev/ min.

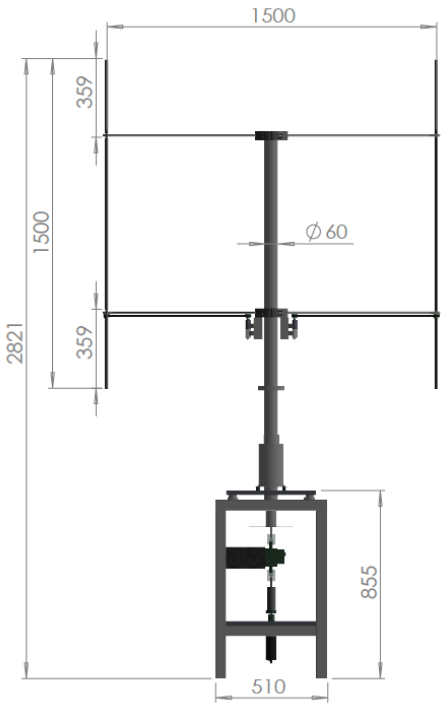

Figure 3. PitchVAWT Turbine

Table 1. PitchVAWT Specifications

Property	**Dimension**
NBlades	2
Height	1.5 m
Diameter	1.5 m
Blade Chord	0.075 m
Strut Chord	0.060 m
Solidity	0.1
Blade Airfoil	NACA0021
Strut Airfoil	NACA0018
TSR	4
U_∞	$4\,\mathrm{m\,s^{-1}}$

3. Modeling of expected behavior

An estimate of the expected turbine loading based upon changes in pitch is modelled using the Actuator Cylinder model [6]. The inviscid formulation of lift and drag ($C_L = 1.11(2\pi)sin(\alpha)$ and $C_D = 0$) is used in the model with an azimuthal step of 5°. The inviscid formulation of the airfoil polar is used in order to divorce the low Reynolds number viscous effects and dynamic stall which are expected in the wind tunnel test from the input of varying the turbine pitch.

3.1. Pitch Schedules

As a proof of concept for influencing the overall thrust vector for the turbine. It is hypothesized that adding a sinusoidal pitch with a phase offset of 90° would cause a sufficient influence in the angle of attack experienced by the blades to shift the overall load vector in the desired direction. Using the Actuator Cylinder model with inviscid polars, simulations were conducted for fixed pitch operation at $\beta = 0$ for a baseline and a 10° sinusoidal curve leading and following the azimuth position of the rotor. Figure 4 gives a representation of the applied pitch as the rotor revolves. The thicker black line represents the zero pitch point.

3.2. Simulation Results

The resultant angle of attack for each simulation is given in figure 5. As can be seen the experienced angle of attack on the blades shifts to a greater value earlier in the rotation for the sinusoidal pitching which is 90° advanced of the rotor position and the opposite pitch has the opposite reaction as expected. This leads to the normal force distributions given in figures 6 and 7. The loads have been normalized by $1/2\rho AU_\infty^2$ and are plotted using the solid red line. The double thick solid black line is used to denote the 0 line. A scaled normal vector is used to show the value at each evaluation point. A single vector in the center of the plot denotes the integrated value over the entire rotation which represents the total force from the rotor onto the flow. As

can be seen from the simulation, the average load vector has indeed shifted approximately 45° from center in each of the sinusoidal cases. Due to the inviscid polar formulations the results of the zero pitch case give an average loading directly facing back into the wind, as to be expected.

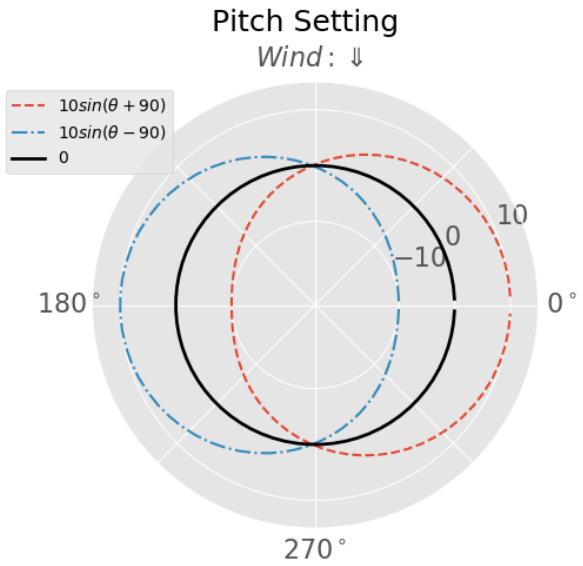

Figure 4. Pitch setting for each azimuth position

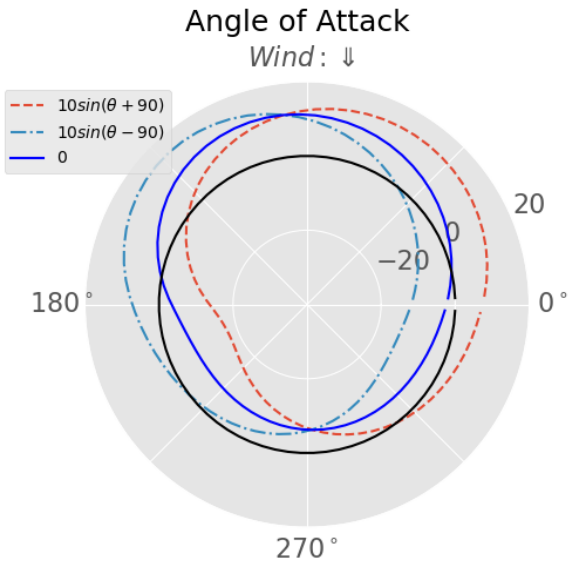

Figure 5. Expected α for each pitch from AC model $C_L = 1.11(2\pi)sin(\alpha)$ $C_D = 0$

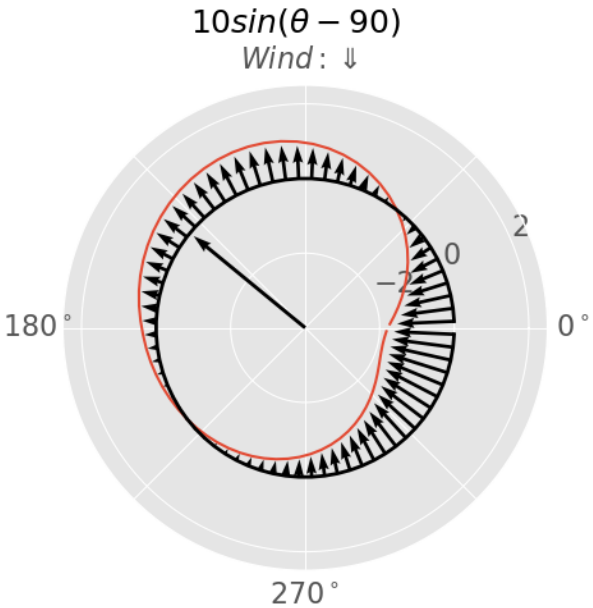

Figure 6. Non-dimensional F_N for inviscid polar with 10° sinusoidal pitch lagging by 90°

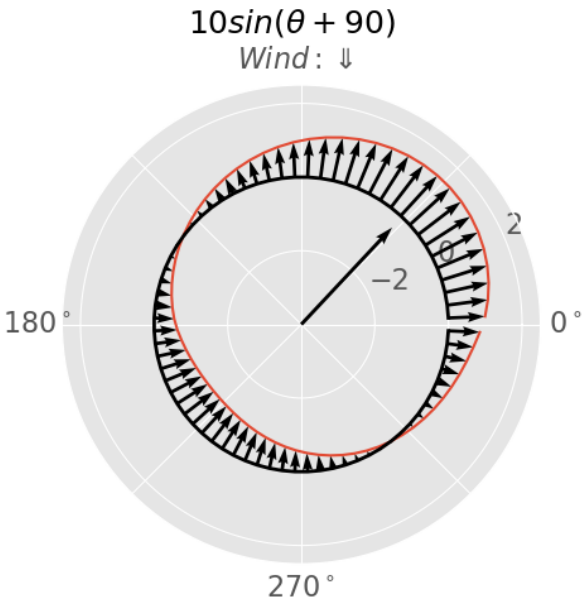

Figure 7. Non-dimensional F_N for inviscid polar with 10° sinusoidal pitch leading by 90°

3.3. Normal Load Assumption

Due to inherent difficulties with directly measuring the tangential loads on each blade, an assumption is made within the apparatus that measuring the normal loading at each azimuth position provides a good representation of the total turbine loading. In order to verify this assumption, turbine thrust is calculated from the AC Model both with and without inclusion of the tangential force vector. Figure 8 and table 2 highlight the effect of ignoring the tangential component of the blade forces on the calculated thrust magnitude and direction. In the direction of the wind, the difference is negligible, however there is a slight underestimation of the cross-flow thrust. This underestimation leads to a offset in calculated thrust direction of approximately $\pm 2.5°$ for the current model across the pitch schemes. This error is considered acceptable for the current analysis. However, depending on the purpose of the study, as in a rotor or platform dynamic model, this may need to be taken into account.

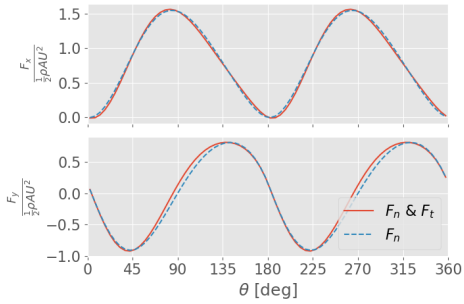

Figure 8. Thrust with and without F_t, $\beta = 0°$

Table 2. Integrated Thrust Values

β	**Param**	**Mag**	**Dir**
$0°$	F_n, F_t	0.843	89.93°
	F_n	0.848	92.58
$10°sin(\theta + 90°)$	F_n, F_t	1.035	39.9°
	F_n	1.05	41.29
$10°sin(\theta - 90°)$	F_n, F_t	1.207	149.1°
	F_n	1.163	146.49°

4. Data collection and processing

Data is collected from a set of sensors on the turbine to determine quantities of azimuth position, blade position, normal blade loading, rotor torque, reaction loads transferred to the tower base, and base accelerations. Data is collected, processed, and stored using National Instruments^{TM}hardware at a rate of 500 Hz. The digital rotary quadrature encoder provides an angular resolution of 0.25° and a rotational speed resolution of 2.5 rot/ min. The data analysed in this paper will be limited to the effects of blade normal loading, however all data can be made available upon contacting the authors.

4.1. Normal load from measured strain on strut

The normal load is measured using a set of strain gages on the top strut of blade 1. The symmetric cross-section for the NACA 0018 strut profile is shown in figure 9. A full-bridge strain gage setup shown in figure 10, is utilized in an axial configuration within a wheat-stone bridge in order to compensate for any vertical bending or temperature fluctuations which can occur while testing. The signals are routed through a data slip ring and into a National Instruments NI9237 strain gage completion module located at the base of the turbine. The output voltage from the wheat-stone bridge is converted to strain using the strain gage equation for the axial configuration of the full bridge and the strain gage factor of 2.13 provided by the manufacturer of the gages, Kyowa. Gage length of each strain gage is 5 mm

The first calculation is to transform the measured strain into a stress. This is performed using Hooke's Law given in equation 2. The measured strain is multiplied by the known elastic modulus of the material (given in table 3). The quantities expressed in the table have been directly measured. For axial loading the stress on a cross section is the force on that section divided by the area, equation 3. For this calculation, the force has only been measured on one of

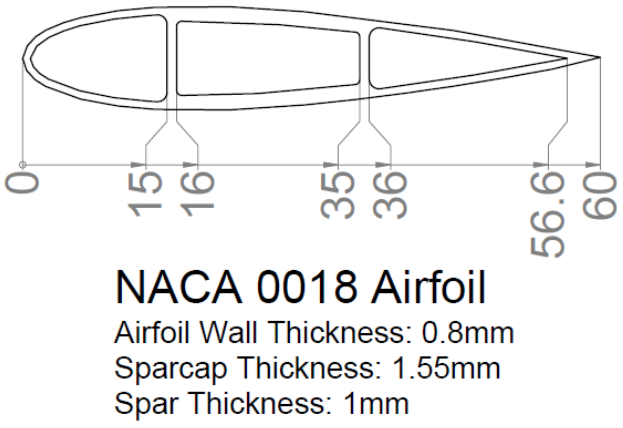

Figure 9. Strut cross-section

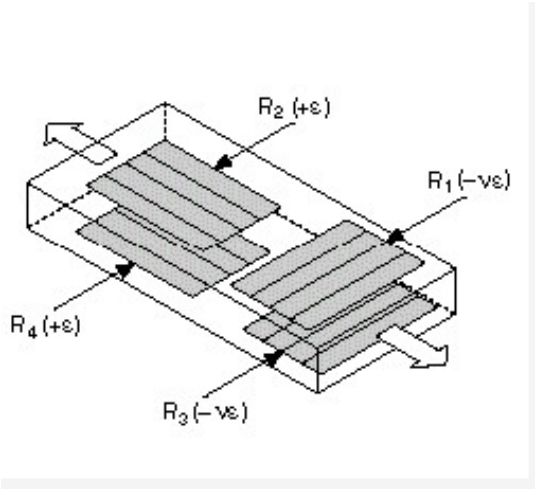

Figure 10. Strain gage configuration for measuring axial strain [7]

Table 3. Strut Material Properties

Property	**Dimension**
ρ_{strut}	$2620\,\mathrm{kg\,m^{-3}}$
E_{strut}	$55\,\mathrm{GPa}$
$A_{cross-section}$	$143\,\mathrm{mm^2}$

the two struts and is therefore doubled, equation 4. Due to the symmetrical design of the blades and struts, the assumption that the normal loading is equally distributed among the struts is considered valid for this exercise. Data is captured on the bottom strut using a quarter-bridge strain gage, which does not compensate for bending or temperature effects, and is not used in this analysis, although is useful in quantifying rotor behavior in other contexts.

$$\sigma_n = E\epsilon_n \tag{2}$$

$$F_{n_{strut}} = \sigma A_{cross-section} \tag{3}$$

$$F_{n_{blade}} = 2F_{n_{strut}} \tag{4}$$

4.2. Post-processing

Several post-processing steps are required to achieve the desired normal load data per azimuth position. The first is to remove the large centripetal load due to the rotation of the turbine. The load increases with the square of the rotational speed and is on the order of 200 N which is approximately an order of magnitude higher than the expected normal load due to the aerodynamics. The load versus the rotational frequency is plotted in figure 11. A second degree polynomial is fit to the curve and used to correct for the rotational load by subtracting the polynomial fit from the measured data. The azimuthally varying load for each rotational speed is preserved.

The next correction to the load is performed by filtering out information which is due to the vibration characteristics of the turbine and due to high frequency noise. Using the rotational speed from the rotary encoder and the known wind velocity, the tip speed ratio is calculated.

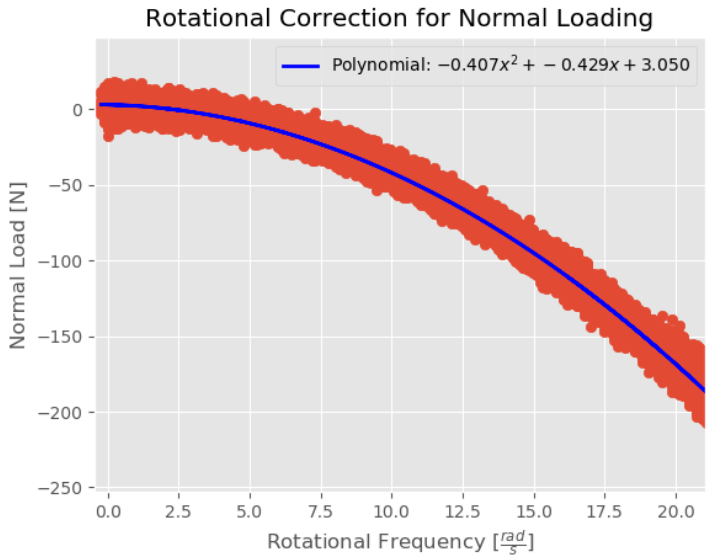

Figure 11. Rotation correction

The data is then filtered to include the desired tip speed ratio for analysis. From this data the 1P excitation frequency is calculated. Frequency content greater than ten times the rotational frequency is removed using a digital low-pass filter. Vibration dynamics of the turbine discussed in a previous paper [8], are modeled using Siemens Nastran. The campbell diagram of the turbine is given in figure 12. At the rotational speed of the testing (205 rev/min), the platform which the turbine is mounted to in the tunnel has substantial motion due to vibration as well as the tower forwards and backwards whirl modes. A power spectrum of the normal load is given in figure 13. Black vertical lines represent excited structural modes of the turbine. These frequencies, especially the tower whirl modes, represent added dynamics in the normal load measurement which are not directly due to the aerodynamics. For this analysis, the load at these specific frequencies is removed using a set of notch filters.

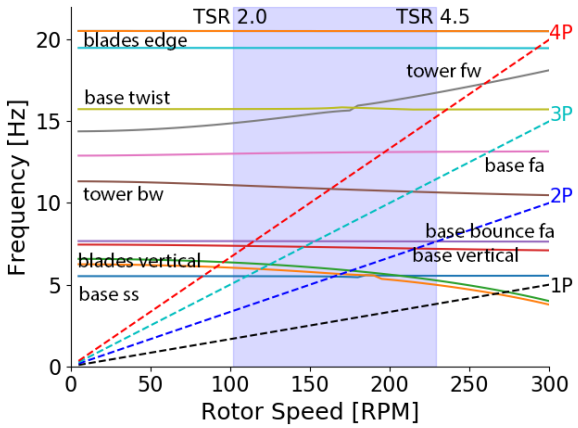

Figure 12. Turbine Campbell diagram, 205 RPM at $\lambda = 4$ where, fa: fore-aft, ss: side-side, fw: forward-whirl, bw: backward-whirl

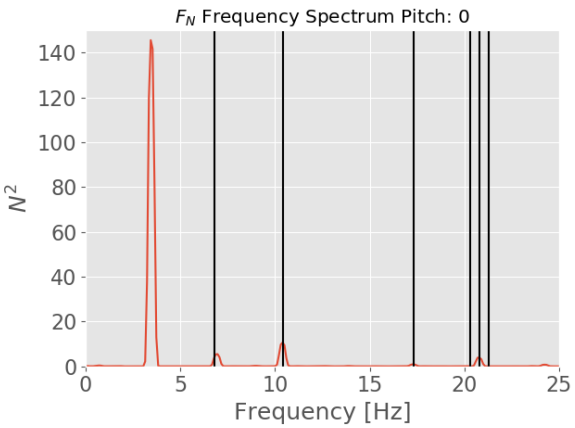

Figure 13. Power Spectrum of unfiltered F_N with vertical lines showing natural frequencies of pertinent modes

The normal load is then segmented into azimuthal bins with a resolution of 5°. Each bin has a minimum of 300 samples. The mean and standard deviation are then calculated for each bin. When plotted in each following figure, the mean is given as a marker, with the vertical lines representing 1 standard deviation for the bin. The normal loads are non-dimensionalized by the rotor area and the incoming wind speed ($1/2\rho AU_\infty^2$).

5. Testing

Turbine testing is performed in the Open Jet Facility at TU Delft. The tunnel has an octagonal outlet measuring 2.85 m by 2.85 m. The center of the wind turbine is placed approximately 2 m from the opening of the tunnel. Wind speeds were held at a constant 4 m s^{-1} as measured by the tunnel control system. The turbine rotational speed was controlled in order to match specific tip speed ratios in increments of 0.5 from 1 to 4. At a tip speed ratio of 4, the experienced chord-wise Reynolds number on the airfoils range from a low of approximately 5.5×10^4 in the pass moving away from the incoming wind to 9.5×10^4 in the upwind pass.

6. Results

The normal force for the blade with a tip speed ratio of 4 is given in figure 14. The upwind pass is fairly smooth with the load beginning to collapse to zero just after the 90° position. The load on the downwind pass, from 180° to 360°, has elements of blade vortex interaction and tower passage which show up in the oscillatory response. The response has been converted into X and Y directional loads and plotted in figure 15. This response is due solely to blade 1. The loading is greater in magnitude and smoother on the upwind pass, as the incoming wind is clean. On the downwind pass, the blade passes through the wake of the first pass, and therefore has a lower wind speed with greater oscillations as to be expected.

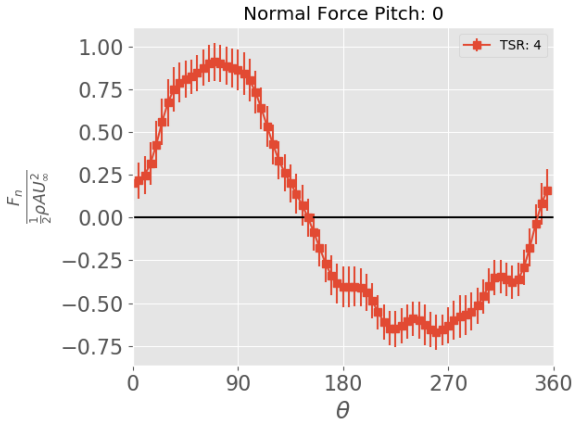

Figure 14. F_n vs θ zero pitch TSR4

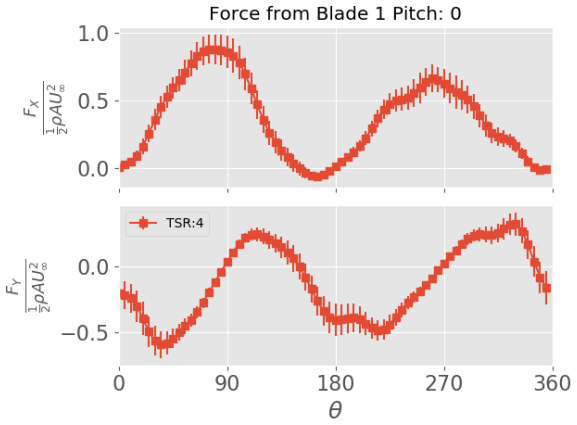

Figure 15. Blade 1 loading composed into X and Y directions

Figure 16 shows the overlay of each normal load distribution versus the azimuth position of the turbine. As hypothesized, the normal blade loads are shifted due to the addition of the sinusoidal blade pitch with the phase offsets. The $10° \sin(\theta + 90°)$ pitch setting causes the peak load to occur earlier in the rotation as the positive pitch setting adds to the increasing angle of attack as the blade enters the upwind rotor position. The $10° \sin(\theta - 90°)$ pitch follows behind the zero pitch load case as the pitching causes the maximum load to occur later in the rotation. Like the above analysis for zero pitch, the loads are converted into X and Y and plotted in figure 17. However, for this comparison, the expected total thrust load is plotted. This is calculated

by sampling the normal loading measured by blade 1 as it would be experienced by blade 2 operating 180° out of phase. This assumes that blade 1 and blade 2 are exactly the same in performance. The peaks in the X direction are offset in azimuth position as expected. Although the vertical shift in the Y direction shows the effect of offsetting the pitch phase the greatest.

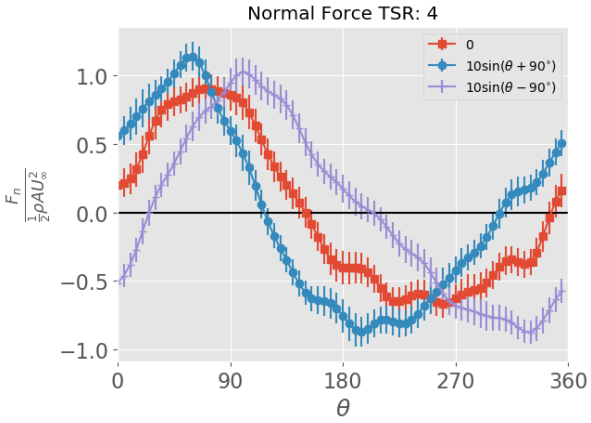

Figure 16. F_n vs θ phased sinusoidal pitch input and zero pitch response

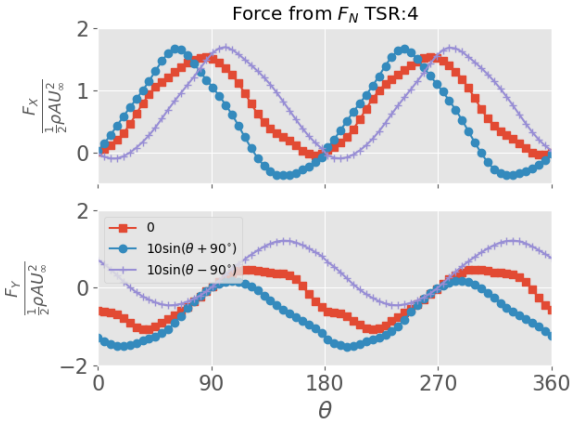

Figure 17. Total X and Y load computed from normal measurement

Figures, 18, and 19 show a polar plot of the normal force coefficient with respect to azimuth position of the blade for each pitch scheme. The oncoming wind is from the 90° position as depicted in the figures. The integrated magnitude and direction of the normal force is given as an arrow from the origin of each polar plot. As shown, the integrated thrust vector changes substantially from the zero pitch response position by the inclusion of both phases for sinusoidal pitch actions showing a swing of 78.9°. This follows the pattern from the expected results calculated with the Actuator Cylinder model. Although the physics occurring within the real turbine loading is more complicated than the model, including three-dimensional effects, low-Reynolds number effects, flow curvature, and unsteady effects, the overall shift in thrust direction were measured.

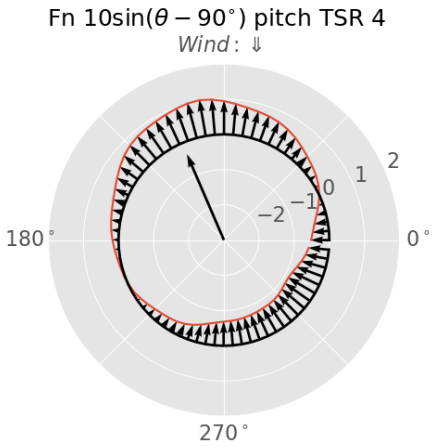

Figure 18. F_n vs θ for pitch 90 degrees lagging rotation θ_{Thrust}: 116.6°

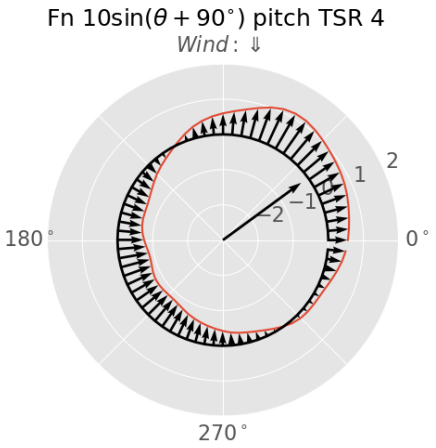

Figure 19. F_n vs θ for pitch 90 degrees leading rotation θ_{Thrust}: 37.7°

A summary of the turbine thrust loading is given in table 4. The direction vector given is

in the coordinate system of the turbine, in the direction of the thrust load onto the flow. With the wind coming out of the 90° azimuth position, the zero pitch thrust response has an offset of about 18° this is most likely due to viscous airfoil effects and the large change in Reynolds number between the upwind and downwind passes. There is also a strong likelihood of unsteady effects and dynamic stall happening after the 90° position. The angular change in thrust position can be easily seen with a shift from this 72° zero pitch response to 117° with the lagging pitch and 38° with leading pitch. The swing represents a change of 78°. The overall magnitude of the thrust vector increased for both the pitching conditions meaning there is a price to pay in blade and thrust loading for deflecting the thrust from the zero pitch position. A study of closed loop control of blade pitch for the purpose of directing this thrust vector would have significant benefits in limiting unnecessary loading.

Table 4. Summary of turbine thrust loading

β	C_{T_X}	C_{T_Y}	**Mag**	**Dir**
0	0.73	0.24	0.76	71.8°
$10°sin(\theta + 90°)$	0.54	0.70	0.88	37.7°
$10°sin(\theta - 90°)$	0.76	−0.38	0.85	116.6°

7. Conclusions

Testing was conducted on a two-bladed H-VAWT wind turbine with actively controlled variable pitch in order to demonstrate the control authority of varying the thrust vector with turbine pitch. Predetermined sinusoidal pitches of $10°sin(\theta \pm 90°)$ were prescribed to the turbine while operating at a tip speed ratio of $\lambda = 4$. The normal force of the turbine was measured and used to determine the overall aerodynamic thrust in X and Y directions of the turbine. The overall magnitude of the thrust vector increased slightly from the zero pitch performance while the direction of the thrust was altered by up to 78°.

References

[1] Huijs F *et al.* 2018 Integrated design of a semi-submersible floating vertical axis wind turbine (vawt) with active blade pitch control (*EERA DeepWind 2018 15th Deep Sea Offshore Wind R&D Conference* vol 1104) (Trondheim, Norway: IOP Publishing Ltd) p 12
[2] Ennis B L and Griffith D T 2018 System levelized cost of energy analysis for floating offshore vertical-axis wind turbines Report Sandia National Laboratories
[3] de Korte B 2019 *Investigating the potential of load and power control on a vawt through active pitch control* Thesis Delft University of Technology
[4] LeBlanc B P and Ferreira C S 2018 Overview and design of pitchvawt: Vertical axis wind turbine with active variable pitch for experimental and numerical comparison AIAA SciTech Forum Wind Energy Symposium (Kissimmee, Florida: American Institute of Aeronautics and Astronautics) p 11
[5] LeBlanc B P and Ferreira C S 2018 Experimental determination of thrust loading of a 2-bladed vertical axis wind turbine (*The Science of Making Torque from Wind* vol 1037) (Milan, Italy: IOP Publishing Ltd) p 9
[6] Madsen A H, Paulsen U S and Vita L 2014 Analysis of vawt aerodynamics and design using the actuator cylinder flow model The Science of Making Torque from Wind (Copenhagen, Denmark: IOP Science) p 11
[7] Instruments N 2019 Measuring strain with strian gages URL `https://www.ni.com`
[8] LeBlanc B P and Ferreira C S 2019 Experimental characterization of h-vawt turbine for development of a digital twin (*North American Wind Energy Association / Windtech* vol 1452) (Amherst, MA, USA: IOP Publishing Ltd)